



Morphology and thermal stability of AlF₃ thin films grown on Cu(100)

G. Ruano^a, J.C. Moreno-López^a, M.C.G. Passeggi Jr.^a, R.A. Vidal^a, J. Ferrón^{a,b,*}, M.Á. Niño^c, R. Miranda^{c,d}, J.J. de Miguel^{d,e}

^a Laboratorio de Superficies e Interfaces, Instituto de Desarrollo Tecnológico para la Industria Química (INTEC, CONICET-UNL), 3000, Santa Fe, Argentina

^b Departamento de Materiales, Facultad de Ingeniería Química, Universidad Nacional del Litoral, 3000, Santa Fe, Argentina

^c IMDEA-Nanociencia, Cantoblanco, 28049, Madrid, Spain

^d Dpto. Física de la Materia Condensada, Univ. Autónoma de Madrid, Cantoblanco, 28049, Madrid, Spain

^e Instituto de Ciencia de Materiales "Nicolás Cabrera", Univ. Autónoma de Madrid, Cantoblanco, 28049, Madrid, Spain

ARTICLE INFO

Article history:

Received 22 September 2011

Accepted 10 November 2011

Available online 18 November 2011

Keywords:

Aluminum fluoride

Insulators

Spintronics

Radiolysis

Electron beam resist

ABSTRACT

The growth of ultrathin epitaxial layers of aluminum fluoride on Cu(100) has been studied by a combination of surface science techniques. Deposition at room temperature results in step decoration followed by the formation of dendritic two-dimensional islands that coalesce to form porous films. Ultrathin layers (up to 2 monolayers in thickness) are morphologically unstable upon annealing; de-wetting takes place around 430 K with the formation of three-dimensional islands and leaving a large fraction of the Cu surface uncovered. Films several nanometers thick, on the contrary, are stable up to ca. 730 K where desorption in molecular form sets on. The effect of electron irradiation on the AlF₃ has also been characterized by different spectroscopic techniques; we find that even small quantities of stray electrons from rear electron beam heating can provoke significant decomposition of the aluminum fluoride, resulting in the release of molecular fluorine and the formation of deposits of metallic aluminum. These features make AlF₃ an interesting material for spintronic applications.

© 2011 Elsevier B.V. All rights reserved.

1. Introduction

Spintronics [1,2] has been a very active area of research in Condensed Matter Physics during the last decade, sparked by the great many applications envisaged for spin-based microelectronics. Due to its longer coherence length and smaller scattering probability as compared to the electronic charge, the use of electron spins to convey information should result in higher carrier mobility and lower energetic consumption.

One of the key requirements for a successful development of this technology is the obtention of materials with high spin polarization that can serve as sources of spin-polarized carriers. For that purpose a great deal of attention is being devoted to diluted magnetic semiconductors (DMS). These materials are typically produced by doping III–V or II–VI semiconductors [3,4] with magnetic impurities, but other insulating or wide-gap semiconductors have also been successfully employed [5–8]. In the case of TiO₂ ferromagnetism has been observed at room temperature when doped with either Fe [9,10], Co [11,12] or Ni [9] in the appropriate concentration range. These materials are also attractive due to their relatively easy integration in the microelectronics industry.

Aluminum fluoride (AlF₃) is a wide-band-gap (10.8 eV) semiconductor [13], with good insulating characteristics and transparent in the visible range. It is also rather inert chemically, which makes it a good passivating agent. These characteristics have made it an interesting material for many different applications, ranging from solar cell technology [13] to molecular biology [14]; it could also become an interesting candidate base material for the fabrication of a DMS. Furthermore, it readily decomposes upon irradiation with low- or mid-energy electrons [15–17], releasing molecular fluorine and leaving a deposit of metallic Al on the substrate. This feature makes AlF₃ an attractive inorganic resist for e-beam nano-patterning techniques [18,19].

No studies are known to us up to this moment regarding possible magnetic applications of AlF₃; nevertheless, a related material such as Al_xFe_{1-x} alloys have awakened lately a considerable attention since their structurally disordered phases are ferromagnetic at room temperature in the concentration range 0.32 < x < 0.5 [20], while the atomically ordered phases are paramagnetic [21]. This opens up the possibility to use Fe-doped AlF₃ matrices to create magnetic nanostructures by means of electron lithography techniques.

A necessary requirement before all these promising perspectives can be realized is to reach an accurate control of the preparation conditions of the AlF₃ films. Metal fluorides have been traditionally prepared by fluorination or other chemical synthesis methods with the aim of obtaining materials with a large surface area for catalysis applications [22]. Nevertheless, the films produced by these methods show

* Corresponding author at: Instituto de Desarrollo Tecnológico para la Industria Química (INTEC, CONICET-UNL), 3000 Santa Fe, Argentina. Fax: +54 342 4550944.

E-mail addresses: jferron@intec.unl.edu.ar (J. Ferrón), juanjose.demiguel@uam.es (J.J. de Miguel).

a high porosity, which precludes most solid state applications. Films grown by DC magnetron deposition show an apparently good homogeneity [23] but only for very high thicknesses; however, no atomic scale characterization of the density of surface defects has been performed on them. The structural and chemical stability of the films is also an issue [24]; several conflicting reports have appeared in the past on this subject [18,25–27], demonstrating the need for a detailed, multi-technique study that can unravel all the subtleties of this interesting system. The purpose of this work is to perform a detailed characterization of the early stages of growth of ultrathin AlF_3 films, their chemical and thermal stability and their response to electron bombardment. A $\text{Cu}(100)$ single-crystal surface was chosen as the substrate for simplicity given its stability and easy preparation.

2. Experimental

The measurements reported in this paper have been performed in three different ultra-high vacuum (UHV) chambers; the availability of common techniques in all of them ensured the reproducibility of the experimental conditions.

An ample combination of different surface science techniques was employed in order to obtain a comprehensive characterization of the growing AlF_3 films. The evolution of their roughness was monitored in real time during deposition by means of thermal energy atom scattering (TEAS). After growth, the surface morphology could be determined in real space by scanning tunneling microscopy (STM), and its crystallinity by low-energy electron diffraction (LEED). The chemical state and metallicity of the films both before and after electron irradiation were then studied by Auger electron spectroscopy (AES), electron energy loss spectroscopy (EELS) and secondary electron emission (SEE).

2.1. Sample preparation

The $\text{Cu}(100)$ single-crystal was cleaned by repeated cycles of Ar^+ sputtering (1 keV , $\sim 5 \mu\text{A}\cdot\text{cm}^{-2}$) and annealing at 800 K until contamination was below the detection limit of AES and a sharp LEED diffraction pattern was observed or, in the system equipped with TEAS, until a good surface reflectivity for the He specular beam ($\geq 30\%$ of the direct beam) was obtained. Under these conditions, atomic resolution could be obtained with STM on the flat terraces without noticeable amounts of contaminants or defects. It has been pointed out in previous reports that AlF_3 surfaces can be easily contaminated by the adsorption of water vapor [22]; this effect is particularly intense for very porous films, which present a large surface area for adsorption of contaminants. As we will demonstrate in the following, one of the main goals of our study is precisely to determine the best preparation conditions to obtain homogeneous, compact films that will be less prone to contamination. Furthermore, and in order to minimize the presence of water vapor in the experimental chamber, anhydrous AlF_3 (CERAC Inc, Milwaukee, WI, USA, 99.5% purity) was grown by thermal evaporation at deposition rates between 2×10^{-2} and $8 \times 10^{-4} \text{ ML/s}$. The Knudsen cell was equipped with a thermocouple allowing us to monitor the crucible temperature, a shutter to precisely control the deposition time and a water-cooled shroud; it was carefully outgassed for several hours before starting the experiments at temperatures slightly above those used during growth. The composition of the residual gas was monitored during outgassing in the UHV systems equipped with a mass spectrometer; under the typical operating conditions only a slight increase in the CO signal could be detected. The pressure in the vacuum chambers was kept in the low 10^{-9} mbar range during evaporation, and fell into the mid 10^{-10} mbar range during the measurements. Unless otherwise indicated, all depositions were done at room temperature or slightly above. The sample was heated by different methods: in general, either radiation or direct heating using a ceramic oven was used to avoid

irradiating the sample with electrons. Rear electron bombardment was used in some cases to test its effects on the AlF_3 films.

2.2. Auger, energy loss and secondary electron emission spectroscopies

These measurements were performed in a UHV surface analysis system with a base pressure in the 10^{-10} mbar range. Differentiated Auger spectra of the F-KLL and $\text{Al-L}_{2,3}\text{VV}$ transitions and energy loss (EELS) spectra were acquired using a single-pass cylindrical mirror analyzer (CMA) with a resolution of 0.6% and 2 V peak-to-peak modulation amplitude. Secondary electron emission (SEE) induced by ion bombardment is a very surface-sensitive technique, its main drawback being its poor chemical selectivity. It is usually employed to gather information on the electronic structure of materials but in this particular case we use it to derive morphological information by characterizing the local environment of the Al atoms. The electron emission was measured with the same energy analyzer but in the integrated mode and with a sample bias of -6 V in order to collect the full spectra, avoiding any work function difference between sample and analyzer. The electron beam had an energy of 2 keV for AES and 100 eV for EELS measurements; its incidence angle was 30° with respect to the surface normal in all cases. Ion-induced electron emission experiments were carried out using a 5 keV Ar^+ ion beam for the excitation. The current density on the sample was kept low enough so as to minimize the effects of irradiation.

2.3. Thermal energy atom scattering

TEAS experiments were carried out in a specially designed UHV system that has been described in detail elsewhere [28]. The sample manipulator allows for direct heating with a ceramic oven and liquid nitrogen cooling. Sample cleaning is accomplished by noble gas sputtering with an ion gun of 3 keV maximum energy, and high-temperature annealing. The system is also equipped with a LEED optics for crystallographic structure characterization.

For the TEAS experiments the monochromatic, neutral He beam is generated by a supersonic nozzle source and modulated by means of a piezo chopper. After scattering at the sample surface, it is detected by a quadrupole mass spectrometer that can be moved inside the UHV chamber; the signal is then fed to a lock-in amplifier tuned to the modulation frequency ($\sim 240 \text{ Hz}$). This technique possesses several advantages for the study of insulating films: besides its extreme surface sensitivity, the use of neutral atoms as a probe suppresses any possible effects due to charging of the substrate and/or damage of the films by irradiation with charged particles. Furthermore, the scattering process being almost purely kinematic facilitates the interpretation of the data using simple but intuitive growth models [28].

2.4. Scanning tunneling microscopy

All STM measurements were carried out at room temperature in a UHV chamber with a base pressure in the low 10^{-10} mbar range. The deposition rate was varied between 2×10^{-2} and $8 \times 10^{-4} \text{ ML/s}$; the deposited coverages were determined by direct analysis of the STM images. Electrochemically etched tungsten tips were used for all STM experiments reported in this work. The polycrystalline W tips were routinely cleaned by Ar^+ ion bombardment and annealing in UHV. All the STM images shown here were acquired at room temperature in the constant current mode with a sample bias voltage of $+2.50 \text{ V}$ and tunneling currents ranging between 0.1 and 0.7 nA . Acquisition and image processing were performed using the WSxM free software [29].

3. Results

3.1. Growth and morphology of thin AlF_3 films

We start by describing the first stages of growth of the AlF_3 films. TEAS allows us to continuously monitor the evolution of the surface roughness by measuring the intensity of the specular He beam during deposition; a characteristic result of such a measurement is illustrated in Fig. 1(a). The monotonic decrease of the surface reflectivity, depicted with black dots, reveals a steady accumulation of disorder as the surface coverage increases. This behavior is usually associated with rough, multilayer growth and slow surface diffusion [28,30]. The specular intensity vanishes for a coverage slightly above 0.5 ML, indicating that the whole surface is more or less uniformly covered by the adsorbate at this stage. The well ordered LEED patterns that were visible on the clean $\text{Cu}(100)$ were completely absent at the end of this deposition, just above 1 ML, thus confirming the rough nature of these films. The evolution of the Auger peak-to-peak intensities, shown in Fig. 1(b), is also characteristic of layer-by-layer growth [31]. The crossing of the decreasing Cu signal and the increasing F intensity reveals that the substrate is being uniformly covered by the adsorbate.

A clearer, albeit static picture of the morphology of the growing AlF_3 film can be gained from STM images. Fig. 2 shows two micrographs of the $\text{Cu}(100)$ surface after deposition of 0.05 and 0.25 ML AlF_3 . Several features deserve being mentioned: In the first place, all

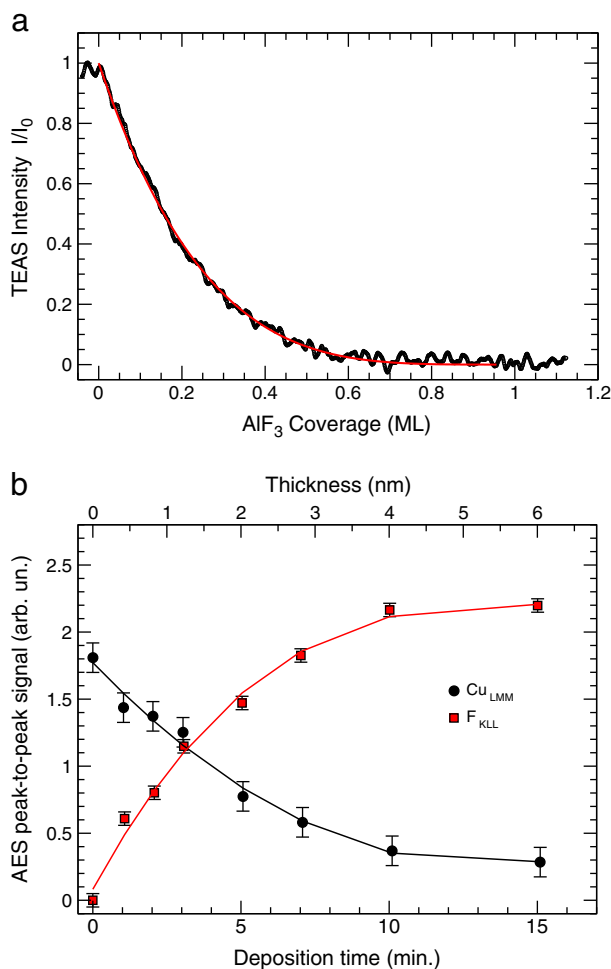


Fig. 1. (a) Evolution of the TEAS specular intensity during deposition of AlF_3 on $\text{Cu}(100)$ at room temperature. The solid red curve is a fit to the data using a random adsorption model (see text for details). (b) Temporal evolution of the F and Cu AES signal during RT deposition of AlF_3 . The solid lines are guides to the eye.

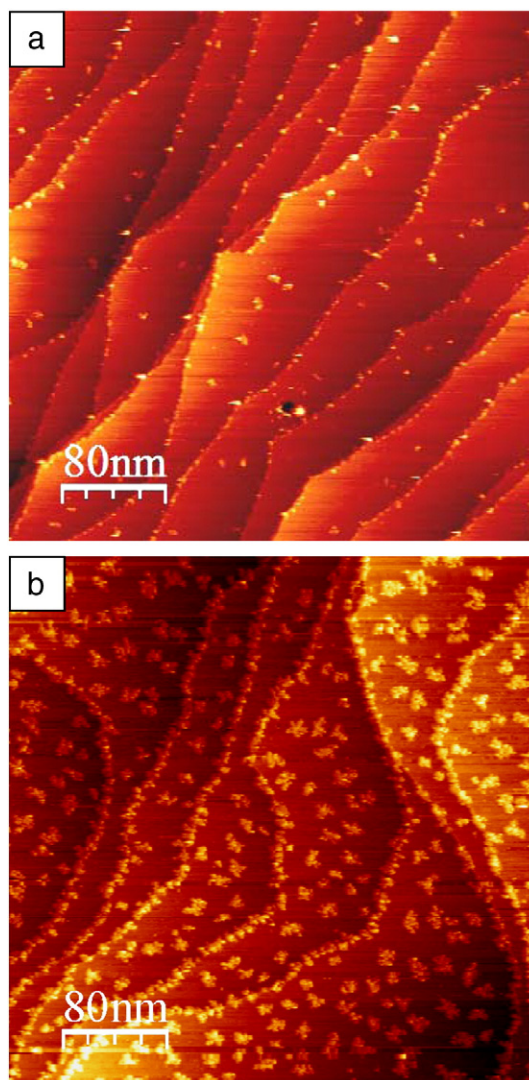


Fig. 2. STM images, 400 nm on both sides, of (a) 0.05 ML and (b) 0.25 ML AlF_3 grown on $\text{Cu}(100)$ at room temperature.

the substrate's atomic steps are decorated by AlF_3 islands, indicating that the diffusion length of the individual molecules after their arrival to the surface is at least as large as the average terrace size [32,33]. Cluster formation at the atomic steps most likely involves some mixing of the aluminum fluoride molecules with the Cu atoms; once that the steps are fully covered with islands nucleation starts across the terraces, indicating that the steps have become passivated and turned into repulsive walls for incoming AlF_3 molecules. An analogous behavior has been reported during the growth of Co on $\text{Cu}(111)$ [34]. The islands formed on the terraces have an approximately dendritic shape that can be ascribed to a diffusion-limited aggregation process in which the AlF_3 monomers become immobilized at the same position where they stick to a pre-existing island [35–37]. This island morphology, with its large perimeter-to-area ratio, explains the high degree of roughness detected by the TEAS experiment depicted in Fig. 1. Based on these observations, we have analyzed those data with a theoretical model that assumes a random adsorption of the growing species on the surface [38–40]. Despite this relatively crude approximation, the data can be well fitted as demonstrated by the solid curve (red, in the online version) shown in Fig. 1(a).

The empty space between the dendrites is difficult to fill by newly arriving molecules, and thus a consequence of this growth mode is the formation of rather porous layers with abundant openings or pin-holes. This feature can become an important shortcoming for the

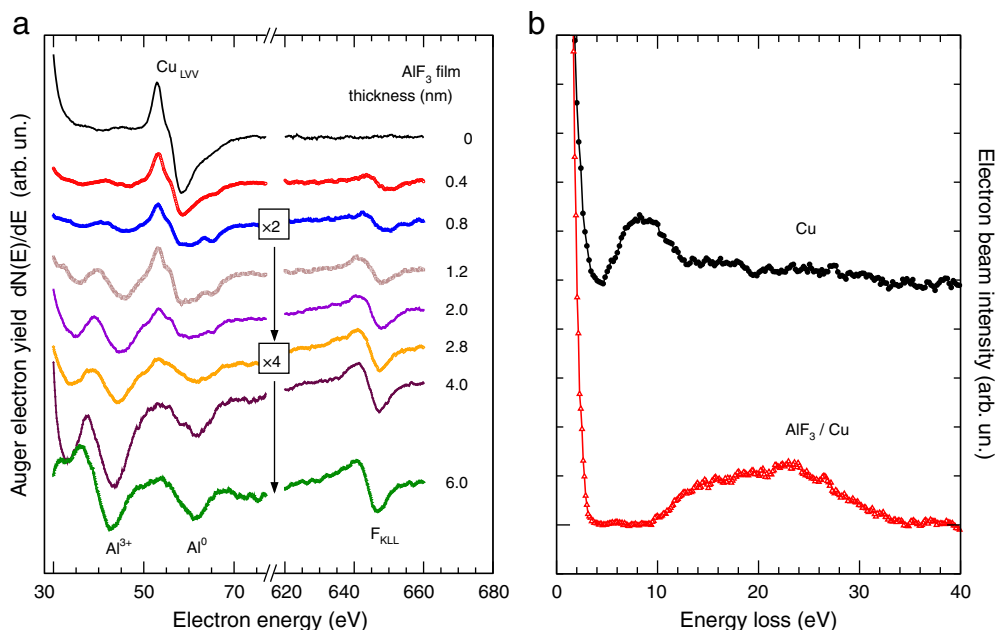


Fig. 3. (a) Series of Auger spectra measured with increasing AlF_3 thickness. (b) Electron energy loss spectra measured on the clean $\text{Cu}(100)$ surface and on a 5 nm thick AlF_3 film.

potential use of AlF_3 layers as insulators. A possible way to improve the film morphology could be to raise the deposition temperature in order to increase edge diffusion and try to promote the growth of more compact layers. Nevertheless, the use of thermal treatments can be problematic; a detailed characterization of the thermal stability of the aluminum fluoride films is therefore clearly needed and it will be the subject of Section 3.2.

The growth of the aluminum fluoride films has also been characterized with Auger spectroscopy. The evolution of the Cu-LVV, Al-LVV and F-KLL Auger line shapes with increasing AlF_3 thickness is presented in Fig. 3(a). The gradual attenuation of the Cu signal and the simultaneous increase of the Al and F ones allow us to calibrate

the deposition rate; the film thicknesses have been determined from our calibration, by measuring the height of the high energy Cu-LMM peak at 920 eV, which has a larger escape depth and can therefore be detected even after deposition of several nanometers of aluminum fluoride. The Al peak shows a large chemical shift of up to 22 eV depending on its oxidation state: it appears at an energy of 43 eV when the Al atom is bonded to the fluorine and at 65 eV when it is in the metallic state. It is noteworthy that, even with the low beam current density employed for these measurements, some metallic Al can always be detected resulting from the electron-induced decomposition of the aluminum fluoride. For this reason in the thermal desorption experiments every data point was acquired

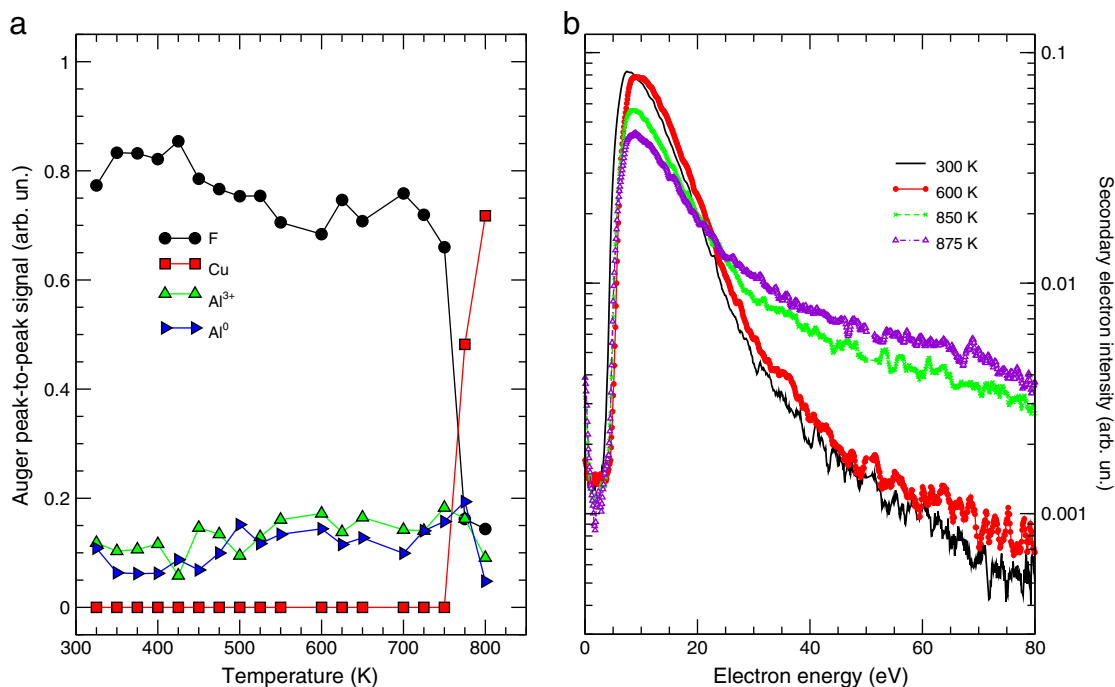


Fig. 4. Thermal evolution of an AlF_3 film studied by (a) AES and (b) SEE under rear radiation heating.

at fresh positions on the sample, not previously irradiated. We shall come back to this issue in more detail in Section 3.4. AES spectra were also used to investigate the presence of contaminants at the sample's surface; negligible amounts of C and O could be detected, which allows us to rule out the possibility of significant adsorption of water from the residual gas in the UHV chambers during the typical time intervals required for performing the experiments (a few hours).

Fig. 3(b) in turn depicts EELS spectra for the clean Cu substrate and a 5 nm thick AlF_3 film. The Cu plasmon peak at 8.5 eV is evident in the first spectrum, but it totally disappears when the substrate is covered by the insulating fluoride layer. In this latter case the spectrum clearly shows a band-gap of ~ 10 eV.

3.2. Thermal stability of AlF_3 layers

Next, we set out to determine the thermal stability of the aluminum fluoride films. In order to avoid any damage caused by the electron bombardment, either radiation from an incandescent filament placed behind the sample or direct heating through a ceramic oven were used for this part of the work. Fig. 4 summarizes the changes suffered by a 15 nm thick AlF_3 film with increasing sample temperature as monitored by AES – panel (a) and SEE – panel (b). The AES data reveal that this relatively thick fluoride film remains both

chemically and morphologically stable up to a temperature of approximately 750 K. Above this limit, the simultaneous decrease of the F and Al signals and the rise of the Cu Auger yield suggest the desorption of the aluminum fluoride without any sign of decomposition.

The secondary electron emission data displayed in Fig. 4(b) provide additional clues regarding the transformations taking place in the AlF_3 film. The high energy tail visible in the spectra at high temperature is characteristic of clean Cu, where a Fermi shuttle mechanism [41] has been proposed to explain this highly energetic emission [42]. The increase in the electron yield in that energy range upon annealing is therefore consistent with the progressive disappearance of the aluminum fluoride from the Cu substrate.

3.3. Effects of temperature on growth kinetics and film morphology

Having demonstrated the thermal stability of the AlF_3 layers against decomposition whenever electron irradiation is avoided, we now turn to characterizing the effect of thermal treatments on the aluminum fluoride films. We focus first on the island morphology. The quasi-dendritic shapes of the islands formed by deposition at RT, already described in Section 3.1, are illustrated clearly in the high resolution STM image of 0.30 ML of AlF_3 presented in Fig. 5(a). Annealing of these islands for 5 min at 500 K results in more rounded perimeters and compact shapes as visible in the micrograph of Fig. 5(b). This implies that, at least for these submonolayer deposits, edge diffusion has been activated at that temperature, allowing the nucleated atoms to move along the steps searching for more favorable sticking positions. It is also noteworthy that the density of islands does not change during annealing, which means that adatom detachment from the islands is not significant at this temperature. Analysis of the island density and its dependence on the deposition rate and the substrate's temperature [43,37] yields an estimated diffusion length of ~ 10 nm for the individual AlF_3 molecules at RT [44].

Not only isolated islands, but also very thin films can still suffer morphological rearrangements during annealing due to their non-compact growth mode described above. This transformation is exemplified by the TEAS data presented in Fig. 6: there the evolution of the specularly reflected He intensity is depicted, first during the evaporation of 1.1 ML of aluminum fluoride onto the Cu(100) surface at RT and then (right-hand side of the plot) during the progressive annealing of this film. At about 430 K a sudden increase of the surface reflectivity indicates that the surface roughness is rapidly decreasing. This temperature range is compatible with the above-described STM observation of island shape rearrangement during annealing. After such a thermal treatment the TEAS intensity saturates at $\sim 55\%$ of the initial value for the clean Cu(100) surface. A LEED measurement performed on this sample after cooling back down to RT shows a

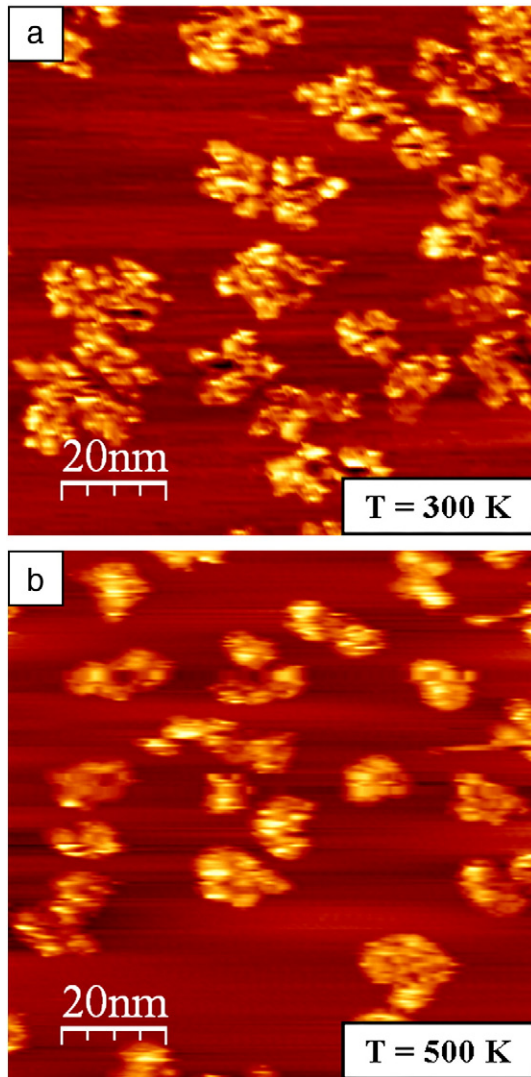


Fig. 5. Blown-up STM images ($100 \text{ nm} \times 100 \text{ nm}$) of 0.30 ML of AlF_3 on Cu(100) acquired at RT and showing detailed views of the island morphologies: (a) As grown at RT, and (b) After annealing at 500 K.

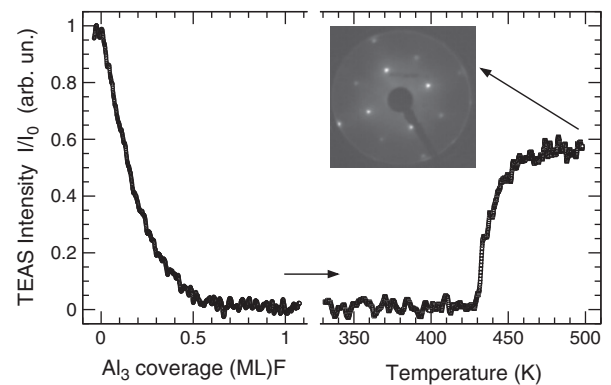


Fig. 6. Evolution of the specular TEAS intensity during deposition of 1.1 ML of AlF_3 at room temperature, followed by annealing up to 500 K. The recovery of specular He intensity at ca. 430 K points out the start of de-wetting. The inset shows the characteristic LEED pattern of Cu(100) visible at 150 eV primary beam energy after annealing.

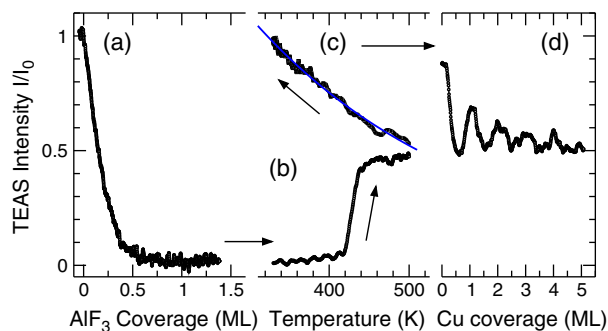


Fig. 7. TEAS experiment illustrating the de-wetting process of a 1.4 ML thick aluminum fluoride film upon annealing. (a) Deposition of AlF_3 at RT; (b) Annealing at 500 K; (c) Cooling down to RT; (d) Deposition of Cu. The blue line in (c) is an exponential fit to the data.

quite sharp pattern corresponding to the clean Cu(100) surface (see the inset in Fig. 6). This means that the thin, rather porous AlF_3 film has agglomerated during annealing, forming compact, probably three-dimensional islands and leaving a large fraction of the Cu surface uncovered. On the contrary, thicker films such as the ones employed for the experiments described in Fig. 4 are morphologically more stable and do not rearrange at such low temperatures.

A further, beautiful demonstration of the partial de-wetting of the Cu(100) surface upon annealing a thin AlF_3 film is provided by the TEAS experiment shown in Fig. 7. There we started by depositing 1.4 ML of aluminum fluoride at RT; the rapid fall of the specular He beam intensity in region (a) of the graph signals the accumulation of roughness in the growing film. After stopping growth, the sample temperature was raised to 500 K – region (b); as in the previous example, the increase in the TEAS intensity marks the break-up and clustering of the AlF_3 layer and the gradual exposure of the underlying Cu substrate. Once that this reordering process was completed, as demonstrated by the stationary TEAS intensity reached near 500 K, the sample was allowed to cool down to RT again in region (c) of the graph. This resulted in a further increase of the reflectivity as a result of the reduced effect of thermal diffuse scattering; the specular TEAS signal roughly follows the exponential law (as demonstrated by the fitting blue line in the figure) dictated by the surface Debye–Waller factor. Finally, we proceeded to evaporate Cu onto

this surface. The intensity oscillations visible in region (d) correspond to the well-known layer-by-layer growth of Cu on Cu(100) at 300 K [45,46]. It is thus evident that the evaporated Cu is growing on top of a mostly uncovered Cu(100) surface.

3.4. Effect of electron bombardment

Finally, we turn our attention towards the effect of electron bombardment on the stoichiometry of the aluminum fluoride films. Fig. 8 shows a temporal series of AES spectra acquired with a primary beam energy of 2 keV and a current density of $20 \mu\text{A}\cdot\text{cm}^{-2}$, which is about 2–3 orders of magnitude lower than the usual values employed in typical AES experiments. In order to determine the effect of the irradiation the beam position was held constant in this case. The first spectrum shows only two Auger peaks at 43 and 650 eV, corresponding to the $\text{L}_{2,3}\text{VV}$ and KLL transitions of oxidized aluminum and fluorine, respectively; no metallic Al can be detected in the fresh sample. With increasing irradiation dose the AES spectra reveal a progressive depletion of fluorine at the surface, accompanied by strong changes in the $\text{Al-L}_{2,3}\text{VV}$ lineshape. The last spectrum in the series shows only metallic Al (at 65 eV) and no traces left of fluorine at the surface.

The extreme sensitivity of the aluminum fluoride to electron bombardment is further demonstrated by the data shown in Fig. 9, which displays the evolution of a 15 nm thick AlF_3 film during annealing by means of rear electron beam heating of the Cu(100) crystal; the energy of the electron beam was 300 eV. The observed behavior is clearly different from that previously presented in Fig. 4 and obtained by means of radiative heating. One can clearly see how even the minor amount of stray electrons reaching the surface is enough to provoke substantial alterations in the film's composition. The Auger measurements in Fig. 9(a) reveal the depletion of F and the appearance of metallic Al^0 , fingerprints of fluoride decomposition, even at RT and growing progressively with annealing temperature. At ~ 575 K the start of Al^0 depletion coincides with a simultaneous steep fall of the Al^{3+} and the appearance of Cu^0 . Since this temperature is substantially higher than the 430 K for which we observed de-wetting in thin films, we conclude that this behavior probably indicates interdiffusion of the metallic Al into the Cu substrate.

Consistently with the AES data, a sharp peak appears in the SEE spectra of Fig. 9(b) at about 65 eV at temperatures between 550 and 600 K. This peak corresponds to the Al-LVV transition arising from the de-excitation of Al^* (carrying an L hole) and taking place outside the solid. This mechanism has been demonstrated by means of Doppler effect measurements [47]. Interestingly, the L hole required to enable this transition is produced by the exciting Ar^+ bombardment in this energy range only through Al-Al symmetric collisions [48]. The appearance of this peak is thus a fingerprint of the aluminum fluoride decomposition and the formation of clusters of metallic aluminum. This peak is absent when the fluoride films are radiatively heated, as shown in Fig. 4(b).

4. Conclusions

The chemical and morphological stability of epitaxial aluminum fluoride films grown on Cu(100) single-crystal surfaces have been characterized by a combination of several surface-sensitive experimental techniques. Submonolayer deposits rearrange upon annealing at ca. 430 K, whereas thicker films are structurally stable up to ca. 760 K, where desorption in molecular form takes place.

Growth of AlF_3 at 300 K results in dendritic island formation. The islands can be made more compact by mild annealing at temperatures not higher than 500 K. AlF_3 , on the other hand, is extremely sensitive to irradiation with medium- or high-energy electrons, which causes molecular dissociation and desorption of fluorine while the Al remains at the surface in metallic form. All kinds of electron beam heating should thus be avoided on handling this material.

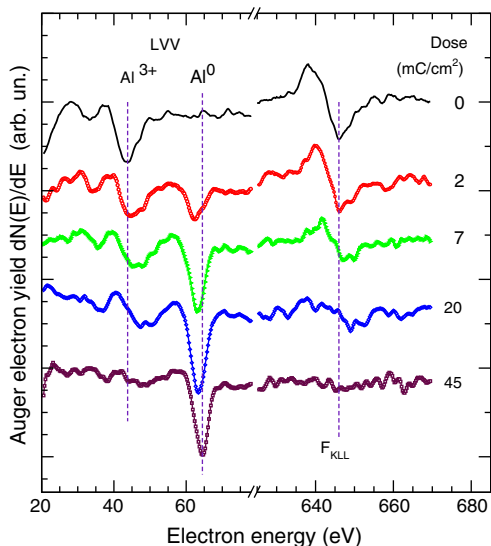


Fig. 8. Progressive reduction of an AlF_3 film by electron irradiation monitored by Auger spectroscopy.

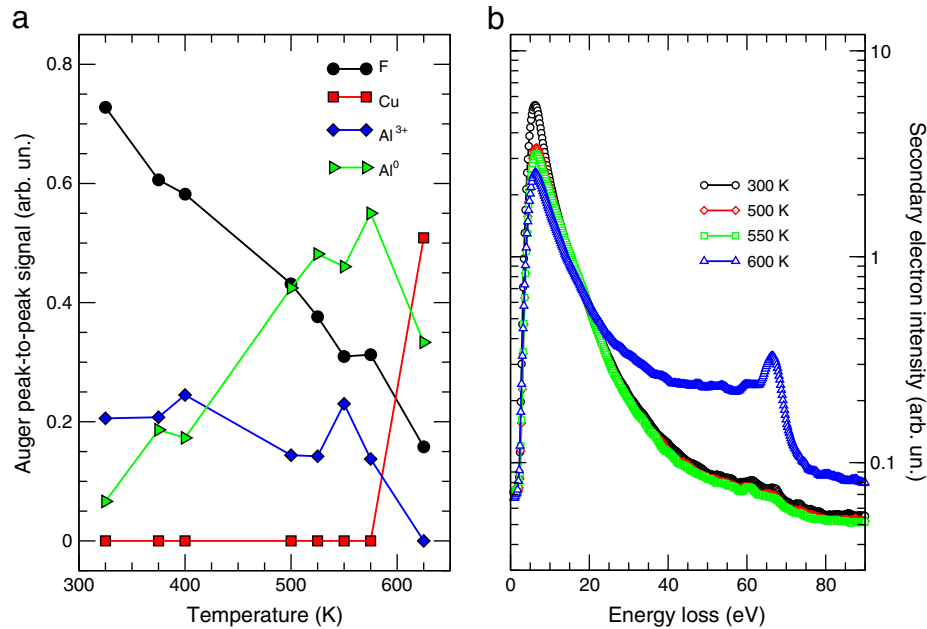


Fig. 9. Thermal evolution of aluminum fluoride studied by (a) AES and (b) SEE under rear electron bombardment heating.

We expect that these findings will constitute a valuable contribution enabling future uses of this material. For most types of applications, ranging from passivating coatings to diluted magnetic semiconductors with possible uses in spintronics, it is necessary to develop preparation methods that allow us to obtain homogeneous films with high structural quality, low porosity and well defined thicknesses. Our results described in this work suggest that compact films can be obtained by thermal evaporation in UHV at substrate temperatures around 400 K, in order to avoid the formation of either the dendritic islands that appear near 300 K or the non-wetting three-dimensional clusters that appear at higher temperature. In all cases, special care must be taken to avoid any electron irradiation of the films, by using either radiative back heating or, preferably, direct sample heating with a resistive oven. Further work is in progress to test the possibility of fabricating a diluted magnetic semiconductor by doping the AlF₃ films with some magnetic (Fe, Co) impurities during growth.

Acknowledgments

This work has been supported in part by the MICINN-Spain through grant FIS2010-18531, by the ANPCyT (PICT 1138/2006 Raíces and 1150/2007), and by the UNL (CAI+D 6-6-62).

References

- [1] G.A. Prinz, *Science* 282 (1998) 1660.
- [2] D.D. Awschalom, M.E. Flatté, N. Samarth, *Sci. Am.* 286 (2002) 66.
- [3] H. Ohno, *Science* 281 (5379) (1998) 951.
- [4] A.H. MacDonald, P. Schiffer, N. Samarth, *Nat. Mater.* 4 (3) (2005) 195.
- [5] M. Venkatesan, C.B. Fitzgerald, J.M.D. Coey, *Nature* 430 (7000) (2004) 630.
- [6] J.M.D. Coey, *J. Appl. Phys.* 97 (4) (2005) 10D313.
- [7] J. Cui, Q. Zeng, U.J. Gibson, *J. Appl. Phys.* 99 (8) (2006) 08 M113.
- [8] W. Prellier, A. Fouchet, B. Mercier, *J. Phys.: Condens. Matter.* 15 (37) (2003) R1583.
- [9] N.H. Hong, J. Sakai, W. Prellier, *J. Magn. Magn. Mater.* 281 (2–3) (2004) 347.
- [10] Z. Wang, W. Wang, J. Tang, L.D. Tung, L. Spinu, W. Zhou, *Appl. Phys. Lett.* 83 (3) (2003) 518.
- [11] Y. Matsumoto, M. Murakami, T. Shono, T. Hasegawa, T. Fukumura, M. Kawasaki, P. Ahmet, T. Chikyow, S.-Y. Koshihara, H. Koinuma, *Science* 291 (5505) (2001) 854.
- [12] W.K. Park, R.J. Ortega-Hertogs, J.S. Moodera, A. Punnoose, M.S. Seehra, *J. Appl. Phys.* 91 (10) (2002) 8093.
- [13] D. König, R. Scholz, D.R.T. Zahn, G. Ebest, *J. Appl. Phys.* 97 (09) (2005) 093707.
- [14] S. Klein, M. Franco, P. Chardin, F. Luton, *FEBS Lett.* 579 (25) (2005) 5741.

- [15] A. Murray, M. Scheinfein, M. Isaacson, I. Adesida, *J. Vac. Sci. Technol. B* 3 (1) (1985) 367.
- [16] W. Langheinrich, B. Spangenberg, H. Beneking, *J. Vac. Sci. Technol. B* 10 (6) (1992) 2868.
- [17] L.I. Vergara, R. Vidal, J. Ferrón, *Appl. Surf. Sci.* 229 (1–4) (2004) 301.
- [18] G.S. Chen, C.B. Boothroyd, C.J. Humphreys, *Appl. Phys. Lett.* 69 (2) (1996) 170.
- [19] E. Kratschmer, M. Isaacson, *J. Vac. Sci. Technol. B* 5 (1) (1987) 369.
- [20] A. Taylor, R.M. Jones, *J. Phys. Chem. Solids* 6 (1) (1958) 16.
- [21] J. Nogués, E. Apiñaniz, J. Sort, M. Amboage, M. d'Astuto, O. Mathon, R. Puzniak, I. Fita, J.S. Garitaonandia, S. Suriñach, J.S. Muñoz, M.D. Baró, F. Plazaola, F. Baudelet, *Phys. Rev. B* 74 (2) (2006) 024407.
- [22] T. Skapin, G. Tavcar, A. Bencan, Z. Mazej, *J. Fluorine Chem.* 130 (2009) 1086.
- [23] B.-H. Liao, M.-C. Liu, C.-C. Lee, *Appl. Opt.* 47 (13) (2008) C41.
- [24] S. Mukhopadhyay, C.L. Bailey, A. Wander, B.G. Searle, C.A. Muryn, S.L.M. Schroeder, R. Lindsay, N. Weiher, N.M. Harrison, *Surf. Sci.* 601 (2007) 4433.
- [25] R.M. Allen, S.J. Lloyd, C.J. Humphreys, in: A.J. Craven (Ed.), *Electron Microscopy and Analysis 1993*, no. 138 in Institute of Physics Conference Series, 1993, pp. 87–90, conference of the Electron-Microscopy-and-Analysis-Group of the Institute-of-Physics: Electron Microscopy and Analysis 1993 (EMAG93), Liverpool, England, Sep. 14–17, 1993.
- [26] V.I. Nikolaichik, *Philos. Mag. A* 68 (2) (1993) 227.
- [27] C.L. Bailey, S. Mukhopadhyay, A. Wander, B.G. Searle, N.M. Harrison, *J. Phys. Chem. C* 113 (2009) 4976.
- [28] J.J. de Miguel, J. Camarero, R. Miranda, *J. Phys.: Condens. Mater.* 14 (2002) 6155.
- [29] I. Horcas, R. Fernández, J.M. Gómez-Rodríguez, J. Colchero, J. Gómez-Herrero, A.M. Baró, *Rev. Sci. Instrum.* 78 (2007) 013705.
- [30] J. Camarero, V. Cros, M.J. Capitán, J. Álvarez, S. Ferrer, M.A. Niño, J.E. Prieto, L. Gómez, J. Ferrón, A.L. Vázquez de Parga, J.M. Gallego, J.J. de Miguel, R. Miranda, *Appl. Phys. A* 69 (1999) 553.
- [31] E. Bauer, J.H. van der Merwe, *Phys. Rev. B* 33 (6) (1986) 3657.
- [32] Z.Y. Zhang, M.G. Lagally, *Science* 276 (5311) (1997) 377.
- [33] J.A. Venables, *Surf. Sci.* 299 (1–3) (1994) 798.
- [34] L. Gómez, C. Slutzky, J. Ferrón, J. de la Figuera, J. Camarero, A.L. Vázquez de Parga, J.J. de Miguel, R. Miranda, *Phys. Rev. Lett.* 84 (19) (2000) 4397.
- [35] H. Brune, *Surf. Sci. Rep.* 31 (4–6) (1998) 121.
- [36] J. Krug, *Adv. Phys.* 46 (2) (1997) 139.
- [37] I.V. Markov, *Crystal growth for beginners: fundamentals of nucleation, crystal growth, and epitaxy*, 2nd edition World Scientific, Singapore, 2004.
- [38] J.J. de Miguel, J. Camarero, R. Miranda, *J. Phys.: Condens. Mater.* 14 (2002) R1063.
- [39] B. Poelsema, G. Comsa, *Scattering of Thermal Energy Atoms*, Vol. 115 of Springer Tracts in Modern Physics, Springer, Berlin, 1989.
- [40] G. Comsa, B. Poelsema, *Appl. Phys. A* 38 (3) (1985) 153.
- [41] E. Fermi, *Phys. Rev.* 75 (8) (1949) 1169.
- [42] G. Ruano, J. Ferrón, *Nucl. Instrum. Methods B* 266 (22) (2008) 4888.
- [43] J.A. Venables, G.D.T. Spiller, M. Hanbücken, *Rep. Prog. Phys.* 47 (1984) 399.
- [44] J.C. Moreno-López, R.A. Vidal, M.C.G. Passaggi Jr., J. Ferrón, *Phys. Rev. B* 81 (07) (2010) 075420.
- [45] J.J. de Miguel, A. Sánchez, A. Cebollada, J.M. Gallego, J. Ferrón, S. Ferrer, *Surf. Sci.* 189/190 (1987) 1062.
- [46] J.J. de Miguel, A. Cebollada, J.M. Gallego, J. Ferrón, S. Ferrer, *J. Cryst. Growth* 88 (1988) 442.
- [47] G. Zampieri, R.A. Baragiola, *Surf. Sci.* 114 (1) (1982) L15.
- [48] R.A. Baragiola, E.V. Alonso, H.J.L. Raiti, *Phys. Rev. A* 25 (4) (1982) 1969.